ISSN 0022-4766, Journal of Structural Chemistry, 2019, Vol. 60, No. 11, pp. 1842-1849. © Pleiades Publishing, Inc., 2019.
Text © The Author(s), 2019, published in Zhurnal Strukturnoi Khimii, 2019, Vol. 60, No. 11, pp. 1916-1923.

TWO NOVEL Ca(II)-CARBOXYLATE COORDINATION POLYMERS: CRYSTAL STRUCTURES AND ANTIMYELOMA ACTIVITY EVALUATION

J. Liang[1], W. Yue[2], Z. Sun[3], and A. Tong[4]*

In this study, two new coordination polymers $[Ca_3(BTB)_2(NMP)_2(H_2O)_2](NMP)(H_2O)_4$ (**1**, H_3BTB = benzene-1,3,5-tribenzoic acid, NMP = N-methyl-pyrrolidone) and $[Ca_3(NTB)_2(DEF)_2(H_2O)_2](DEF)(H_2O)_4$ (**2**, H_3NTB = 4,4′,4″-nitrilotribenzoic acid, DEF = N,N-diethyl-formamide) based on the alkaline earth metal Ca(II) ion and two rigid C_3-symmetric tricarboxylic acid ligands are successfully prepared via the solvothermal reaction. The structural analysis of complexes **1** and **2** demonstrates the existence of different topologies and structures in the as-prepared complexes because of the conformational flexibility of the organic ligands and the diverse geometry of the Ca(II) based 1D secondary building unit. The particle sizes of these two complexes could be conveniently downsized in nanometer region via a simple treatment. In addition, in vitro anticancer activity of compounds **1** and **2** in nanometer has been studied for inhibition human myeloma cell growth via the 3-(4,5-dimethyl-2-thiazolyl)-2,5-diphenyl-2-H-tetrazolium bromide (MTT) assay.

DOI: 10.1134/S0022476619110192

Keywords: Ca(II)-coordination polymer, single crystal, nanoparticles, myeloma, MTT assay.

INTRODUCTION

Although great achievements have been achieved in the field of biomedicine and chemical synthesis in the past few decades, cancer is still one of the most notorious diseases that kill millions of people every year [1]. In this case, continuous efforts have been paid to find better and more effective drugs for cancer treatment. For the being now, the metal-based complexes that formed by the connection of metal ions with the organic ligands via the coordination bonds have been widely explored as anticancer reagents with cisplatin, carboplatin, and oxaliplatin as the representatives, but these complexes usually suffer from several shortcomings, such as drug resistance and high toxicity [2-4]. Therefore, efforts to overcome these shortcomings have encouraged scientists to fabricate diverse analogs, which are not only valuable for obtaining anticancer drugs with better therapy efficiency, but also for providing useful tools for probing the relationship between structure and anticancer activity [5].

As a new class of organic-inorganic hybrid material composed of multidentate organic ligands as connectors and metal ions/clusters as nodes, coordination polymers (CPs) or metal-organic frameworks (MOFs) combining the advances of

[1]Department of Emergency, 3201 Hospital, Hanzhong, Shaanxi, China. [2]Department of Medical-Record, First People′s Hospital of Jining City, Jining, Shandong, China. [3]Department of Emergency, Binzhou People′s Hospital, Binzhou, Shandong, China. [4]Department of Orthopedics, Yan′an People′s Hospital, Yan′an, Shaanxi, China; *an_tong666@126.com.
Original article submitted March 31, 2019; revised April 26, 2019; accepted May 27, 2019.

both inorganic and organic components have received huge development during the past twenty years [6-8]. The large surfaces, adjustable functionalities and controlled morphology of CPs have resulted in their booming development which could be applied as functional materials in many important domains such as drug delivery, gas storage/separation and biomedicine [9]. Recent studies have revealed that some CPs could be used as anticancer reagents, which show the metal and morphology-dependent anticancer activity [10]. The metal ions in CPs can replace other important metals in enzymes of cancer cells, which may inhibit the growth of cancer cells. Moreover, CPs can impose noncovalent interactions with the DNA molecules of cancer cells though groove binding and intercalation, which might also contribute to the growth inhibition of cancer cells [11]. Many CPs have been reported to show anticancer activities in vitro and in vivo which even perform better than the famous anticancer drug cisplatin [12]. Compared with the widely explored transition metal CPs (such as Ni^{2+} and Co^{2+}), the main group metal-based CPs (such as Ca^{2+} and Mg^{2+}) are less studied as anticancer reagents although they are more biocompatible. On the other hand, the organic ligand plays an important role in the final transportation efficiency of the anticancer reagents across the cell membrane, which is highly associated with the targeted biological activity. In this work, we employ two tridentate organic ligands with the C_3-symmetry, 4,4′,4″-nitrilotribenzoic acid (H_3NTB), and benzene-1,3,5-tribenzoic acid (H_3BTB), to build main group metal-based CPs based on the following considerations. First, the unique molecular symmetry for the H_3BTB and H_3NTB ligands make them ideal connectors in the field of CP chemistry which could result in highly symmetrical 3D networks [13]. Second, the H_3BTB and H_3NTB ligands have great potential for the formation of cage- or channel-type CPs, which are the key features of porous CPs that could be applied in various fields [14]. For instance, Chen et al. have successfully developed new Li(I)-based CP with the H_3NTB ligand, which could be applied in the detection of the Fe(III) ion [15]. Kitagawa and co-workers have reported Ba(II)-based CP based on the H_3BTB ligand, which shows a robust microporous character after the guest removal process. In this study, two new Ca(II)-based CPs $[Ca_3(BTB)_2(NMP)_2(H_2O)_2](NMP)(H_2O)_4$ (**1**, H_3BTB = benzene-1,3,5-tribenzoic acid, NMP = N-methyl-pyrrolidone) and $[Ca_3(NTB)_2(DEF)_2(H_2O)_2](DEF)(H_2O)_4$ (**2**, H_3NTB = 4,4′,4″-nitrilotribenzoic acid, DEF = N,N-diethyl-formamide) have been successfully synthesized by the solvothermal reaction of $CaCl_2$ and two rigid C_3-symmetric tricarboxylic acid ligands (Fig. 1). The structural analysis of complexes **1** and **2** demonstrate the existence of different topologies and structures in the as-prepared complexes because of the conformational flexibility of the organic ligands and the diverse geometry of the Ca(II)-based 1D secondary building unit. Complex **1** is a three-dimensional framework based on the Ca(II)-based 1D rod-like chains connected via the BTB^{3-} ligands with 1D rhombus channels along the axis. The structure of complex **2** could be viewed as the connection of Ca3 clusters via the NTB^{3-} ligands to afford a (4,6,7)-connected net. Furthermore, the size of both CPs could be downsized into the nanosized region via a reflux treatment. In addition, the cytotoxic properties of the two nanosized structures against human myeloma cell lines have been evaluated via the MTT assay.

EXPERIMENTAL

Apparatus and materials. All the chemicals and reagents in this research were commercially available and used as received. The IR spectra (400 ~ 4000 cm^{-1}) were collected using a Brucker Equinox-55 spectrophotometer. An elemental Vario EL III analyzer was used to obtain the C,H,N contents in both complexes. Powder X-ray diffraction (PXRD) profiles

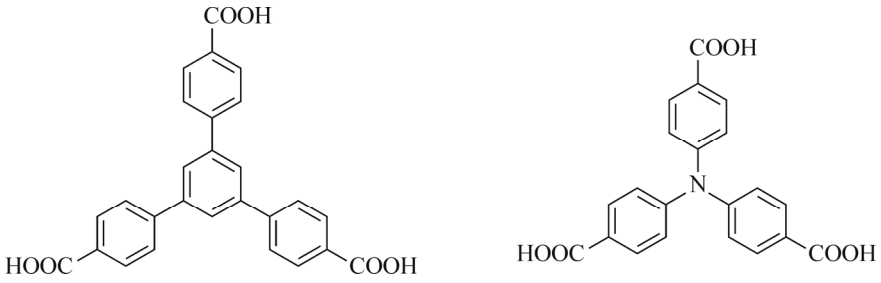

Fig. 1. The chemical drawings of the H_3BTB and H_3NTB ligands used in this work.

were collected using an X′Pert PRO (PANalytical) powder diffractometer with CuK_α radiation. An SDT Q600 (Shimadzu) analyzer was used to record the TGA curves under the nitrogen flow with a heating rate of 10 °C per minute.

Synthesis and characterization of compounds 1 and 2. The synthesis of complex **1** follows a modified synthesis operation reported in the literature [17]. H_3BTB (0.050 g, 0.115 mmol), $CaCl_2$ (0.034 g, 0.30 mmol), N-methyl-pyrrolidone (7.5 g) and H_2O (1.5 g) were mixed and the mixture was stirred for half an hour. The resulting homogeneous mixture was then transferred to a 25 mL Teflon-lined stainless steel autoclave and heated at 120 °C for five days. Needle-like colorless crystals were obtained upon cooling the mixture to room temperature as described above. Yield: 82% based on H_3BTB used. Analytically found for compound **1** ($C_{69}H_{69}Ca_3N_3O_{21}$), %: C 59.12, H 5.03, N 2.96. Calculated, %: C 59.34, H 4.98, N 3.01. FT-IR (cm^{-1}): 3258 (w), 3054 (w, br), 1628 (s), 1539 (m), 1418 (s), 1379 (s), 1355 (s), 1211 (m), 1121 (m), 1024 (m), 900 (w), 799 (s), 774 (m), 709 (m), 693 (s), 629 (m).

H_3NTB (0.043 g, 0.115 mmol), $CaCl_2$ (0.034 g, 0.30 mmol), N,N-diethyl-formamide (6.2 g) and H_2O (0.9 g) were mixed and the mixture was stirred for half an hour. The resulting homogeneous mixture was then transferred to a 25 mL Teflon-lined stainless steel autoclave and heated at 100 °C for three days. Block colorless crystals were obtained upon cooling the mixture to room temperature as described above. Yield: 61% based on H_3BTB used. Analytically found for compound **2** ($C_{57}H_{69}Ca_3N_5O_{21}$), %: C 53.23, H 5.64, N 5.29. Calculated, %: C 53.47, H. 5.43, N 5.47. FT-IR (cm^{-1}): 3279 (w), 2921 (m), 2848 (m), 1621 (s), 1541 (m), 1428 (s), 1391 (s), 1359 (s), 1200 (w), 1023 (w), 899 (w), 801 (w), 772 (s), 716 (m).

Crystal structure determination. Single crystals of compounds **1** and **2** suitable for single crystal X-ray diffraction were carefully picked from the mother liquor with the aid of an optical microscope. The raw data on **1** and **2** were collected using the Oxford Xcalibur E diffractometer and reduced using the CrysAlisPro software. The SADABS system was used to apply empirical absorption corrections. The structural models were established by the direct method using the SHELXS program and refined by full-matrix least-squares method on F^2 using the SHELXL program. All the hydrogen atoms attached to carbon atoms were fixed at their ideal positions, and all non-hydrogen atoms of **1** and **2** were refined anisotropically. Pertinent crystal data and structural refinement results for compounds **1** and **2** were summarized in Table 1. CCDC numbers: 1875013 (**1**) and 1875014 (**2**).

TABLE 1. Crystal Data and Structure Refinements for Compounds **1** and **2**

Compounds	**1**	**2**
Empirical formula	$C_{64}H_{48}Ca_3N_2O_{15}$	$C_{52}H_{50}Ca_3N_4O_{16}$
Formula weight	1205.28	1107.20
Temperature, K	293(2)	293(2)
Crystal system	Monoclinic	Orthorhombic
Space group	*C*2/*c*	*Pbcn*
a, Å	9.8508(4)	23.4838(6)
b, Å	30.192(2)	14.0931(4)
c, Å	29.1803(18)	15.9286(4)
β, deg	96.013(4)	90
V, Å^3	8631.0(9)	5271.7(3)
Z	4	4
ρ_{calc}, g/cm^3	0.928	1.395
μ, mm^{-1}	0.239	0.387
Reflections collected	14470	22056
Independent reflections	6301 [R_{int} = 0.0264]	6141 [R_{int} = 0.0296]
Data / restraints / parameters	6301 / 0 / 381	6141 / 1 / 342
GOOF on F^2	1.079	1.056
Final *R* indexes ($I \geq 2\sigma(I)$)	R_1 = 0.0492, wR_2 = 0.1352	R_1 = 0.0494, wR_2 = 0.1238
Final *R* indexes (all data)	R_1 = 0.0608, wR_2 = 0.1432	R_1 = 0.0675, wR_2 = 0.1340
Largest diff. peak / hole, e/Å^3	0.35 / –0.23	0.79 / –0.66

Antitumor activity. The MTT assay was carried out according to the reported procedures [18-20]. Typically, three human myeloma cells (MM1S, RPMI-8226 and ARH-77) were grown in a RPMI 1460 medium supplemented with 10% fetal calf serum, 100 μg/mL penicillin, and 100 μg/mL streptomycin. They were incubated at 37 °C in a moist incubator and 95% air and 5% CO_2. Cells at the exponential growth were diluted to $5 \cdot 10^4$ cells/mL with RPMI1640, and then seeded in a 96-well cell culture at a volume of 100 μL per cell, respectively, and incubated at 37 °C for 24 h in 5% CO_2. After the incubation of cells for up to 96 h, medium was removed from each cell and 150 μL of an MTT (0.5 mg/mL) solution, diluted 10-fold by RPMI 1460 was subsequently added. The IC_{50} values were measured by depicting the viability to concentration ratio on a logarithmic chart and reading off the concentration where 50% of viable cells were involved in the control. In order to get the mean values, it is requested that each experiment was conducted at least three times in the same way.

RESULTS AND DISCUSSION

Molecular structure. Solvothermal synthesis has been employed for the preparation of the two frameworks described in the present study since this synthetic protocol not only increases the solubility of the as-synthesized complexes, but also often favors an ordered molecular self-assembly. The structural analysis of **1** by single-X-ray diffraction reveals that it belongs to the monoclinic space group *C*2/*c* which possesses a non-interpenetrated three-dimensional network with one-dimensional rhombus channels in each net. The asymmetric part of the unit cell consists of one and a half crystallographically unique Ca(II) ions, one fully deprotonated BTB^{3-} ligand, one coordinated water and one coordinated NMP molecule. The Ca1 atom, sitting on the 2-fold axis, is eight-coordinated with carboxylic O atoms from six different BTB^{3-} ligands; the Ca2 atom with a full occupancy is seven-connected with five carboxylic O atoms on six different BTB^{3-} ligands with the remaining two sites finished by two O atoms from the coordinated water and NMP molecules (Fig. 2*a*). The Ca–O bond distances are in the range 2.343(2) Å to 2.802(2) Å, which correspond to the normal values of reported Ca(II)-based CPs. The adjacent Ca(II) ions are held together via the carboxylic groups of the BTB^{3-} ligands to give rise to a 1D rod-like secondary building unit (SBU) chains along the *a* axis with the Ca1–Ca2 separation of 3.642(3) Å. Each BTB^{3-} ligand binds with seven different Ca^{2+} ions through two different coordination modes, which can be described as $(\eta^1\text{–}\eta^2)\text{–}(\eta^1\text{–}\eta^1)\text{–}(\eta^2\text{–}\eta^2)\text{–}\mu_7$ (Fig. 2*b*). The 1D Ca(II)-based infinite chains are interconnected by BTB^{3-} linkers in the *bc* plane, which leads to the formation of a three-dimensional network with one-dimensional rhombic pores along the *a* direction. The terminally coordinated aqua and NMP molecules are directed towards the pore interior, thus blocking the pores to some extent (Fig. 2*c*). The total solvent accessible volume for **1** is 3663.4 $Å^3$, corresponding to 42.3% of the unit cell volume. The TOPOS analysis indicates that the net of **1** could be viewed as a three-nodal 5,6,7-connected network with the point symbol of $\{3.4^7.5^4.6^8.8\}2\{3^2.4^6.5^2\}2\{4^{10}.5.6^4\}$ (Fig. 3*d*).

The single crystal X-ray analysis reveals that compound **2** crystallizes in the orthorhombic space group *Pbcn* and has a cluster-based three-dimensional network. Its asymmetric unit contains one and a half crystallographically unique Ca(II) ions, one fully deprotonated NTB^{3-} ligand, one coordinated water molecule, and one coordinated DEF molecule. The two Ca(II) ions in **2** adopt different coordination modes. The Ca1 atom has a half occupancy and is eight-coordinated with eight carboxylic O atoms from six different NTB^{3-} ligands to form CaO_8 polyhedral units; while the coordination surrounding of Ca2 is completed by five O atoms from four different NTB^{3-} ligands and two O atoms from the coordinated water and DEF molecules to form a CaO_7 polyhedral unit (Fig. 3*a*). These polyhedral units are linked through edges to form the trimeric Ca_3O_{22} cluster with the Ca1–Ca2 separation of 3.5378(5) Å. There is one NTB anion present in the structure that binds with seven Ca ions using its three carboxylic groups whose coordination mode could be described as $(\eta^1\text{–}\eta^2)\text{–}(\eta^1\text{–}\eta^2)\text{–}(\eta^1\text{–}\eta^2)\text{–}\mu_7$ (Fig. 3*b*). The connectivity in **2** between the trimeric Ca_3O_{22} cluster and NTB^{3-} anions gives rise to a three-dimensional structure (Fig. 3*c*). Due to the closely packed structure of **2** and a relatively large molecular volume of the DEF molecule, complex **2** shows no solvent-accessible free volume as calculated via the software PLATON. The topological analysis with the TOPOS software identified that the structure had a new topological network with a 3-nodal net, a 4,6,7-connected net, which can be presented as the Schläfli symbol $\{4^{10}.6^5\}\{4^4.6^2\}_2\{4^9.6^9.8^3\}_2$ (Fig. 3*d*).

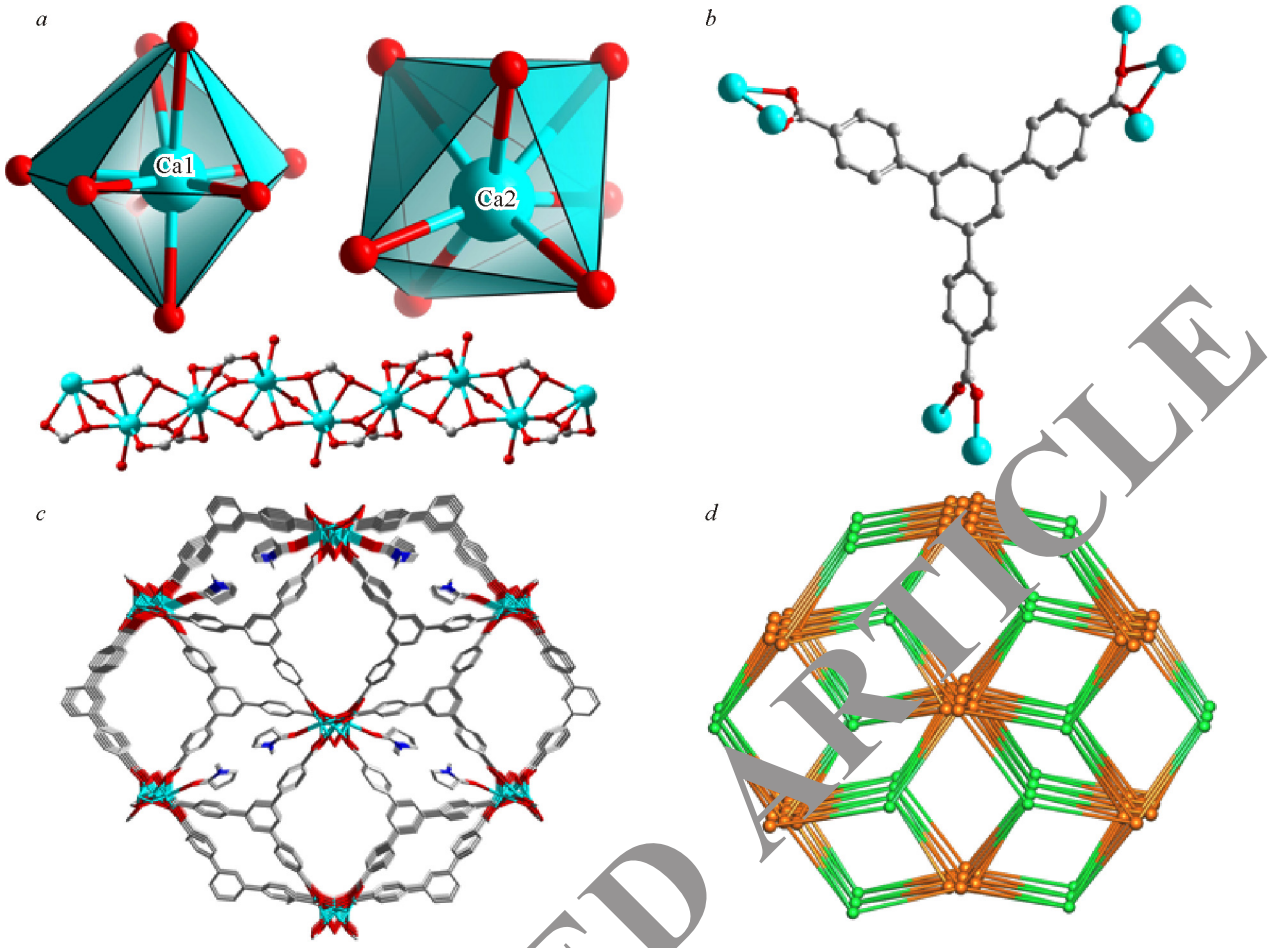

Fig. 2. View of the coordination environments of the Ca(II) ion in **1** (*a*); view of connecting mode for the BTB^{3-} ligand (*b*); view of the 1D rhombic channels of **1** along the *a* axis (*c*); the 5,6,7-connected network for **1** (*d*).

PXRD, TGA and SEM characterization. To character the phase purity of as-prepared two CPs **1** and **2**, their powder X-ray diffraction (PXRD) patterns were recorded using their crystalline samples at room temperature and the profiles were plotted in Fig. 4*a*. The PXRD profiles for the as-prepared samples show sharp peaks, reflecting their high crystallinity. For CP **1**, the experimental diffraction patterns have a group of strong peaks in the range 25-30°, while they are absent in the simulated curve. This discrepancy might be due to the following reason: in the as-prepared samples of **1**, there exist many NMP and water solvent in the lattice, but their electronic contribution was removed from the crystal data by the squeeze option in PLATON. Even if NMP and water crystal solvents are disordered in the voids, their electron density still contributes to diffraction, thus resulting in the additional peaks in the patterns of the as-prepared samples [21-23]. For CP **2**, the experimental diffraction patterns agree with those of simulated ones regarding to the peak positions. The peak intensities in the range 6-7 might be attributed to the preferred orientation of the crystallographic plane [24]. To study the thermodynamic stability of the two compounds, TGA was carried out at a heating rate of 10 °C per min in the temperature range from 25 °C to 800 °C under the continuous nitrogen flow. Complex **1** reveals a sustained weight loss of 28.8% in the temperature range from 25 °C to 501 °C, corresponding to the removal of solvent molecules (both coordinated and uncoordinated lattice solvent molecules). After the loss of guest solvents, a sharp weight loss could be observed, indicating the collapse of the framework. For complex **2**, a continuous weight loss of 16.9% could be observed from room temperature to 487 °C, corresponding to the escape of a half of lattice DEF molecules, two coordinated H_2O and two lattice H_2O molecules. Below that temperature, the framework began to decompose (Fig. 4*b*).

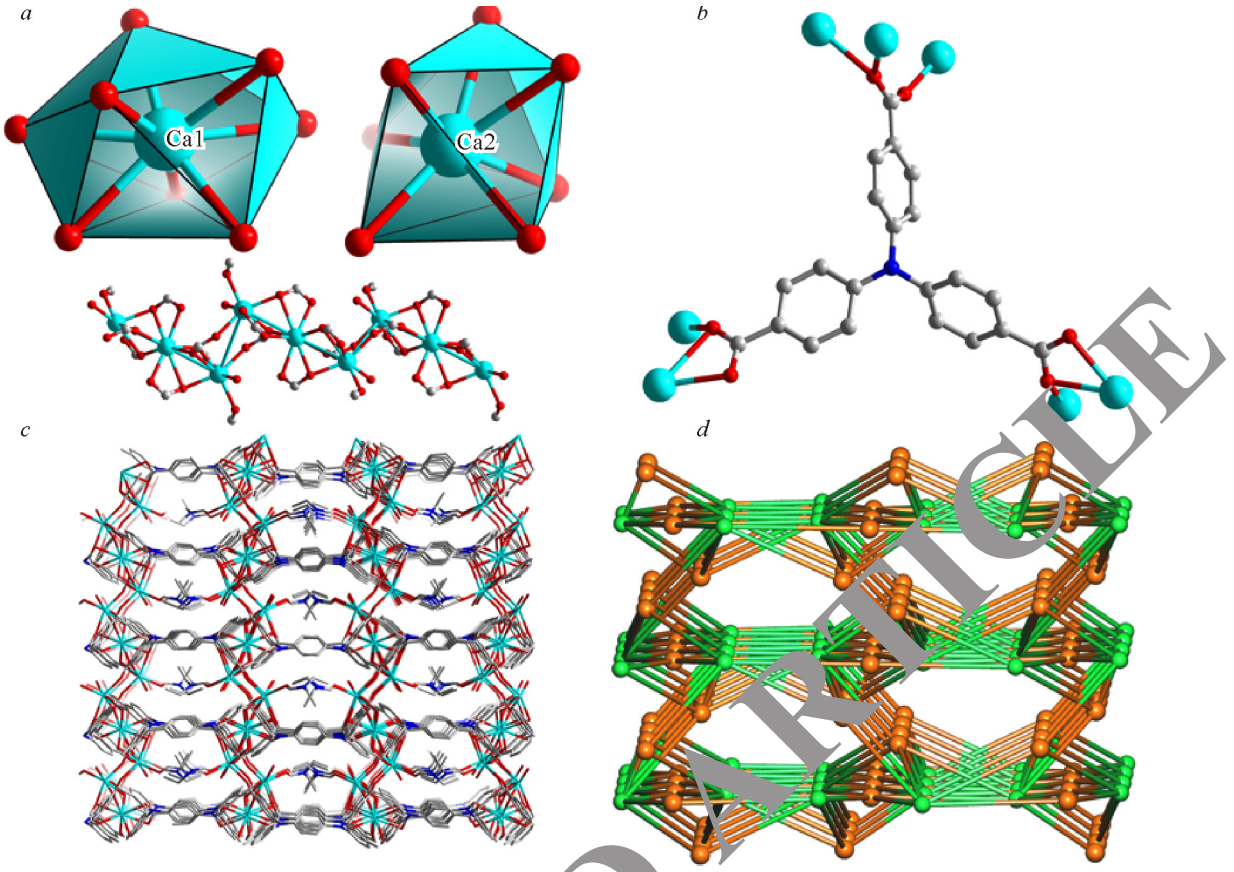

Fig. 3. View of the coordination mode of Ca(II) ion in **2** (*a*); views of coordinating mode of the NTB^{3-} ligand (*b*); view of three-dimensional framework of **2** (*c*); view of the simplified network of **2** (*d*).

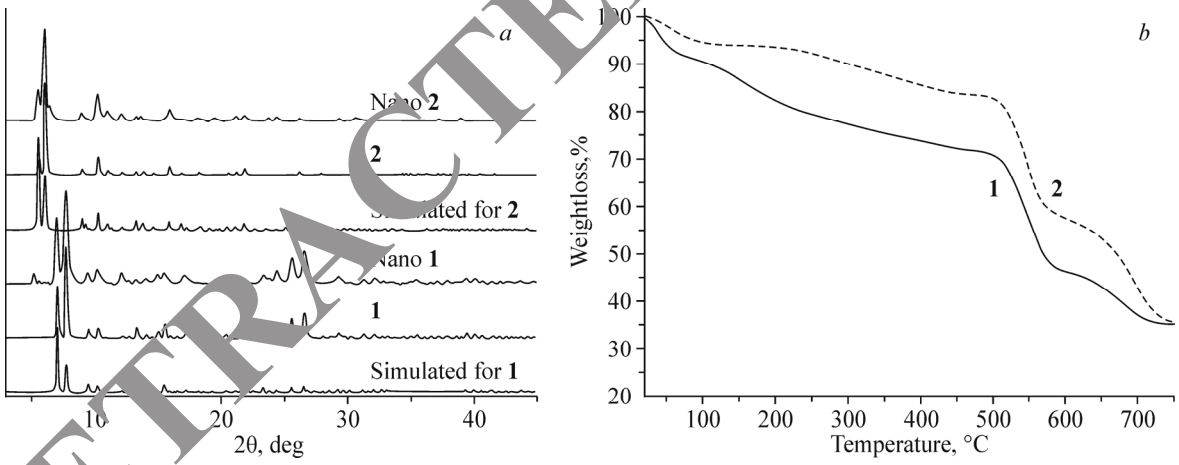

Fig. 4. PXRD profiles for complexes **1-2** (*a*); TGA profiles for complexes **1-2** (*b*).

Considering the following biomedical application, it is necessary to downsize the particles of two CPs to the nanometer scale. Generally speaking, nanoscale CPs could more easily pass though the cell membrane of targeting cancerous tissue and be absorbed by cancerous tissues via the intravenous injection. In a typical experiment, a DMF solution of the organic ligand was added to an aqueous solution combining $Ca(CH_3COO)_2$. After vigorous stirring at 25 °C for 120 min, EtOH was injected into the solution to produce a light-yellow precipitate. SEM images revealed spherical nanoparticles with an average diameter of 110±17 nm (nano **1**) or 94±11 nm (nano **2**), confirming the successful formation of the nanoparticles (Fig. 5). Furthermore, the nano **1** and nano **2** maintained their structural integrality as formed, according to the PXRD measurements.

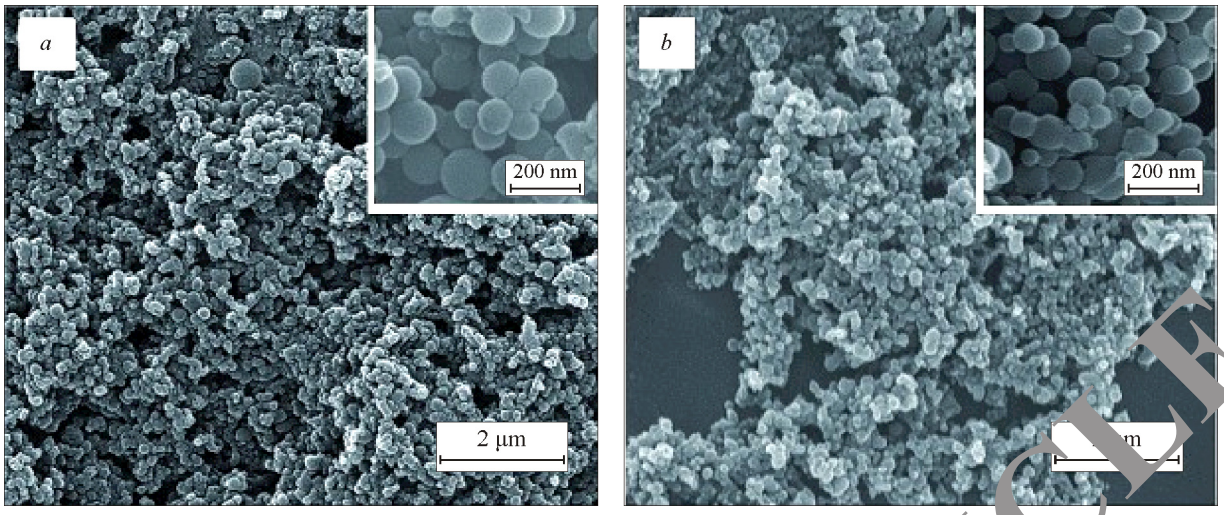

Fig. 5. SEM images of **1** (*a*) and **2** (*b*) nanoparticles showing a good homogeneity and a narrow size distribution.

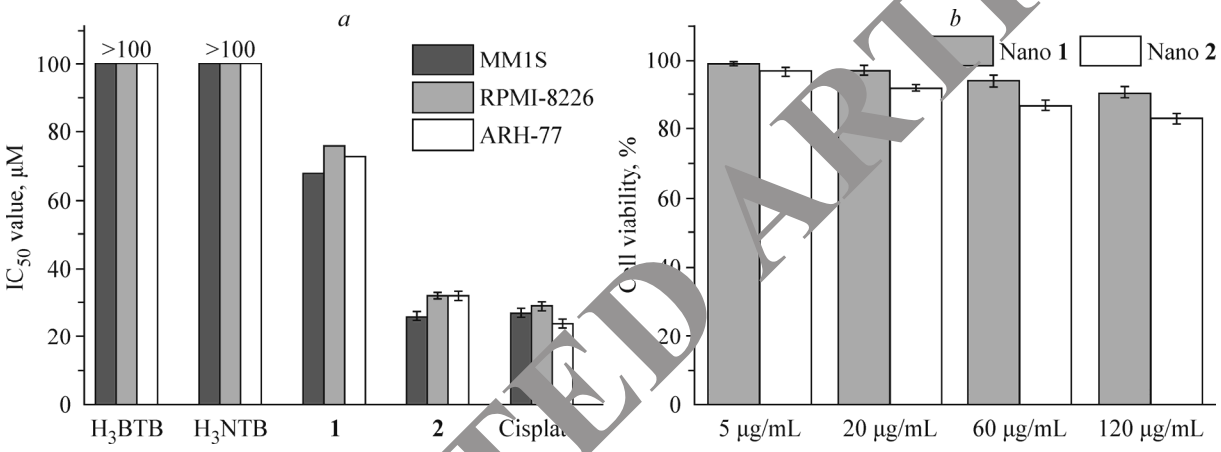

Fig. 6. Growth inhibitory effects of H_3BTB, H_3NTN, nano **1-2** and cisplatin on MM1S, RPMI-8226, and ARH-77 cancer cells (*a*); cell viabilities of the oral epidermal cells after incubation with nano **1-2** at different concentrations (*b*).

Anticancer activity. The cytotoxicities of two nanostructures **1** and **2** along with the organic H_3BTB and H_3NTB ligands against three human myeloma cell lines (MM1S, RPMI-8226, and ARH-77) were studied via the standard MTT assay with cisplatin as the positive control. Fig. 6*a* shows the IC_{50} (half maximum inhibitory concentration) values calculated using the experimental data. It could be observed that no obvious anticancer activity was found for the two organic ligands against all these cell lines because all their IC_{50} values are far above 100 μM. Under the concentration of 100 μM, H_3BTB and H_3NTB should show high cytotoxicity toward all the three cancer cell lines, therefore, it could be inferred that the organic ligands did not show any anticancer activity towards these cell lines.

In comparison, after compounds nano **1-2** were incubated with the cancer cells for three days, the calculated IC_{50} values from the experimental data for these compounds were in the range from 86 μM to 29 μM, indicating that nano **1** and nano **2** showed the anticancer activity toward the MM1S, RPMI-8226, and ARH-77 cells in different degrees. It could be observed that nano **2** shows lower IC_{50} values compared with those of nano **1**, which are even comparable with the famous anticancer drug cisplatin. The present results indicate that the organic ligand has a great effect on the biological activity of resulting CPs. To study the cytotoxicity of nano **1** and nano **2** toward the human normal cell lines, these complexes were incubated with oral epidermal cells (normal cells) for 24 h at different concentrations (0-120 μg/mL), and the cell viability was plotted in Fig. 6*b*. It could be easily read out that even at a concentration of 120 μg/mL of nano **1-2**, the cell viabilities all

remained above 80%. Consequently, it could be concluded that nano **1** and nano **2** demonstrated negligible cytotoxicity toward the human normal cell lines.

CONCLUSIONS

In summary, we successfully prepared two Ca(II)-based CPs by the reaction of $CaCl_2$ and two rigid C_3-symmetric tricarboxylic acid ligands under solvothermal conditions. The structural analysis of complexes **1** and **2** demonstrates the existence of different topologies and structures in the as-prepared complexes because of the conformational flexibility of the organic ligands and diverse geometry of the Ca(II)-based 1D secondary building unit. Their nanoscale samples have been studied for the inhibition of human myeloma cell growth via the MTT assay, which revealed that the organic ligand had a great effect on the biological activity of resulting CPs.

CONFLICT OF INTERESTS

The authors declare that they have no conflict of interests.

REFERENCES

1. A. C. Mertens, Y. Yasui, J. P. Neglia, J. D. Potter, M. E. Nesbit, K. Ruccione, W. A. Smithson, and L. L. Robison. *J. Clin. Oncol*., **2001**, *19*, 3163.
2. Y. Y. Yang, L. Kang, and H. Li. *Ceram. Int*., **2019**, *45*, 8017.
3. Y. Yang, H. Li, W. Zheng, Y. Bai, Z. Liu, and J. Zhang. *Sci. Adv. Mater*., **2019**, *11*, 208.
4. L. Niu, J. L. Xu, W. L. Yang, C. H. Kang, J. Q. Ma, and J. Q. [illegible]. *Sci. Adv. Mater*., **2019**, *11*, 466.
5. H. T. Zhao, X. L. Mu, C. H. Zheng, S. J. Liu, Y. Q. Zhu, [illegible] Gao, and T. Wu. *J. Hazard. Mater*., **2019**, *366*, 240.
6. Y. Feng, H. Fan, Z. Zhong, H. Wang, and D. Qiu. *Inorg. Chem*., **2016**, *55*, 11987.
7. Y. Feng, M. Li, H. Fan, Q. Huang, D. Qiu, and H. [illegible]. *Dalton Trans*., **2015**, *44*, 894.
8. C. Duan, H. Zhang, F. Li, J. Xiao, S. Luo, and H. Xi. *Soft Matter*, **2018**, *14*, 9589.
9. C. Duan, F. Li, M. Yang, H. Zhang, Y. Wu, and H. Xi. *Ind. Eng. Chem. Res*., **2018**, *57*, 15385.
10. L. Kang, H. L. Du, X. Du, H. T. Wang, W. L. Ma, M. L. Wang, and F. B. Zhang. *Desalin. Water Treat*., **2018**, *125*, 296.
11. S. E. H. Etaiw, A. S. Sultan, and A. [illegible] Badr El-din. *Eur. J. Med. Chem*., **2011**, *46*, 5370.
12. S. Shen, Y. Wu, K. Li, Y. Wang, J. Wu, T. Zeng, and D. Wu. *Biomaterials*, **2018**, *154*, 197.
13. H. Furukawa, M. A. Miller, and O. M. Yaghi. *J. Mater. Chem*., **2007**, *17*, 3197.
14. E. Y. Lee, S. Y. Jang, and M. P. Suh. *J. Am. Chem. Soc*., **2005**, *127*, 6374.
15. D. M. Chen, J. Y. Tian, and C. S. Liu. *Inorg. Chem. Commun*., **2016**, *68*, 29.
16. M. L. Foo, S. Horike, and S. Kitagawa. *Inorg. Chem*., **2011**, *50*, 11853.
17. K. S. Asha, M. Mukkitaya, A. Sirohi, L. Yadav, G. Sheet, and S. Mandal. *CrystEngComm*., **2016**, *18*, 1046.
18. L. Duan, K. Zhang, Y. Wang, J. Jin, J. Xie, X. Luo, and Q. Deng. *Inorg. Nano-Metal Chem*., **2018**, *48*, 257.
19. N. Liu, [illegible] Ding, L. Wang, H. Zhao, L. Zhu, and X. Geng. *Brazilian J. Med. Biol. Res*., **2017**, *51*, 1859.
20. B. [illegible] Song, C. Li, and G. F. An. *J. Inorg. Organomet. Polym. Mater*., **2018**, *28*, 1859.
21. [illegible] Glomb, D. Woschko, G. Makhloufi, and C. Janiak. *ACS Appl. Mater. Interfaces*, **2017**, *9*, 37419.
22. S. [illegible] Glomb, G. Makhloufi, I. Gruber, and C. Janiak. *Inorg. Chim. Acta*, **2018**, *475*, 35.
23. M. Y. Sun and D. M. Chen. *Polyhedron*, **2018**, *147*, 80.
24. Z. Karimi and A. Morsali. *J. Mater. Chem. A*, **2013**, *1*, 3047.